Deep Mining 2010 — M. Van Sint Jan and Y. Potvin (eds)

Simulating fault slip areas of mining induced seismic tremors using static boundary element numerical modelling

G.F. Hofmann *AngloGold Ashanti Limited, South Africa*

L.J. Scheepers *AngloGold Ashanti Limited, South Africa*

Abstract

Two mining induced tremors that occurred in a South African deep-level gold mine are considered, with the aim to simulate the shear slip area and source mechanism using static boundary element numerical modelling. Large seismic tremors, induced by the extraction of the tabular ore body typically 1 m high over horizontal spans of kilometres, are a major seismic hazard in South African gold mines. For the cases considered here, virgin stress levels are approximately 54 MPa, and seismic related damage is mainly due to geological faults failing in shear under gravitational loading. The tremors occurred approximately 2 km below surface, 700 m apart in space, and in consecutive months. Seismic recordings and underground observations suggested that the tremors, of local magnitudes 3.0 and 4.0 respectively, were associated with normal slip on similar geological faults. A boundary element numerical model was implemented to some degree of accuracy, since the fault geometries could be inferred from extensive mining spans and fault intersections, and an in situ stress state could be estimated from other available information. Furthermore, the rock mass stress changes and associated surface stress changes on faults could be modelled from monthly measured advance of the mining excavations. Simulation of the seismic sources entailed finding appropriate Mohr–Coulomb strength parameters to allow yielding of the faults at the actual mining stage, and quantitatively in agreement with the seismic moment as inferred from seismic waveform recordings. A critical input into the model was the use of non-zero cohesion in addition to friction angle as specified in the Mohr-Coulomb shear failure criterion, allowing the simulation of co-seismic slip. Hence the breaking of fault cohesion and subsequent stress transfer to the surrounding fault area is simulated, albeit statically, conforming to the perceived triggering of mining related seismic tremors by induced stress changes. The back analysis furthermore suggested that co-seismic stope closure can comprise a significant part of the total recorded seismic moment, depending on the proximity of the hypocentre to mining excavations. From the back analysis a modelling methodology and input parameters are proposed, aiming at identifying vulnerable mining excavations subject to seismic hazard posed by geological structures, hence providing relevant knowledge towards safer mining.

1 Introduction

A back analysis of two large seismic tremors at Great Noligwa Mine in 2009 was done using a boundary element numerical modelling program (the 'Fault Slip' version of Map3D, Wiles, 2010). The objective was to establish whether a boundary element program could successfully simulate shear slip seismic sources, and if so, to establish a forward modelling methodology towards safer mining in the underground tabular mining environment.

The seismic events of interest were of local magnitudes 3.0 and 4.0 respectively, at different stoping areas and in consecutive months (15 October and 29 November 2009). Although the seismic location in elevation is in general subject to error, the location in plan suggests that the events were associated with two faults of the so-called Zuipings type. These are prominent faults at Great Noligwa Mine, dipping shallowly to the north-west (around 50°), with throws typically between 100 and 500 m, and perceivably pose a significant seismic hazard under the extensive mining spans. Both stoping areas were visited shortly after the occurrences, and significant damage was observed in access ways as well as active working places. Although no direct evidence of slip (striations or fault-offset) was observed at the areas visited, the damage was consistent with significant movement on the Zuipings type faults, resulting in severe shakedown damage for both seismic events in proximity to the faults, and also stope closure with the M4.0 event.

As part of the back analysis, evidence of the in situ stress state was gathered, from the literature and underground observations at GNM, and a model input stress state was derived to be used in the boundary element model containing the mining and geological structure geometries. Calibration entailed finding appropriate fault strength properties simulating co-seismic fault slip along the fault boundary elements in correlation with the recorded seismic event magnitudes and locations.

2 Observations and recorded seismic data

2.1 Historical seismicity

Historical seismic data was assembled from seismic systems dating back to 1972. Although there is no guarantee of the completeness of data, it is the best data base available and provides information on large seismic tremors. Figure 1 is a plot and listing of the data for the area of interest. Due to seismic location error and lack of underground damage information there usually is ambiguity regarding the sources of seismic events, especially for the earlier times when fewer seismic sensors were installed. However, for the area of interest the plot suggests that large events are associated with mining abutments coinciding with prominent faults. The locations of some events (e.g. numbers 12, 16) cannot readily be explained, but the majority of events shown are apparently associated with a particular type of fault orientation found in the mine, i.e. faults dipping shallowly to the north. These are named the 'Zuipings faults', with one of these indicated in Figure 1 ('Zuipings-A Fault'). The seismic locations hence suggest shear slip on these faults as the source mechanism.

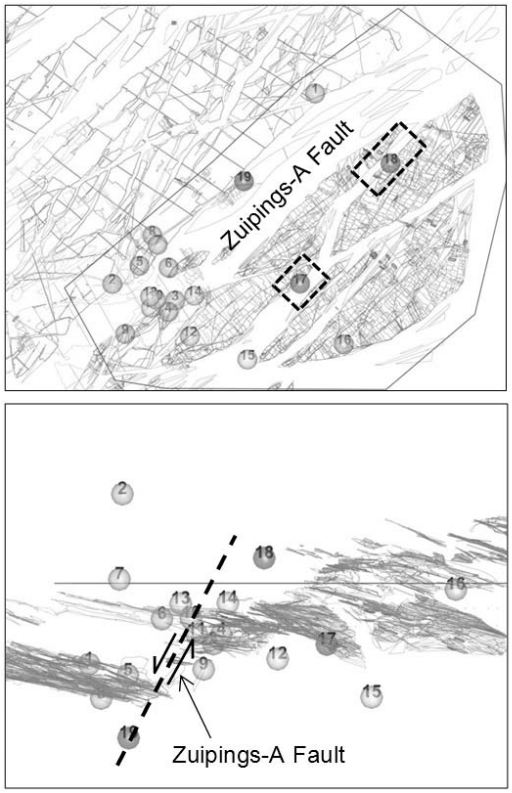

No.	Date	Mag	Ntrigs
1	04 Sep 1992 23:30:00	3.9	10
2	24 Apr 1993 08:21:25	3.0	9
3	10 Mar 1994 23:24:36	3.1	9
4	25 Jul 1994 23:30:53	3.3	8
5	19 Nov 1994 19:43:03	3.3	11
6	27 Nov 1994 13:28:09	3.1	11
7	09 May 1995 08:14:09	3.0	10
8	31 Jul 1995 03:12:59	3.4	10
9	07 Mar 1996 02:28:26	3.2	7
10	25 Apr 1996 09:21:01	3.2	8
11	17 Mar 1998 21:49:55	3.7	13
12	23 Mar 1998 17:12:34	3.5	9
13	21 May 1998 18:14:54	3.4	6
14	13 Jun 1998 23:35:38	3.0	7
15	18 Feb 1999 19:49:24	3.2	4
16	25 Jan 2005 20:10:35	3.9	16
17	15 Oct 2009 16:07:54	3.0	17
18	29 Nov 2009 03:04:49	4.0	18
19	15 Feb 2010 23:09:19	4.1	18

Figure 1 Plan and section views of the area of interest, showing all recorded seismic events since 1972, local magnitude > 3.0. Seismic events numbered 17 and 18 are considered here, with the mining areas and geological faults of interest outlined. The so-called 'Zuipings-A Fault' indicated is one of the typical faults on the mine, believed to be the sources of large seismic events

Of interest here are the seismic events numbered 17 and 18 causing considerable damage. All large seismic events recorded since 1972 are shown, with the first recorded in this area in 1992, suggesting that these events were the first to occur along the faults where they did, and hence providing suitable data for calibration.

2.2 Seismic source analysis from waveform recordings

2.2.1 Location

Location of seismic events in the tabular mining environment suffers from the planar network arrays (seismic stations restricted to within typically 10 m from the tabular ore body, with horizontal mining spans of several kilometres), yielding large location errors perpendicular to the ore body, i.e. approximately in the vertical direction. Locations in plan for the seismic events considered here should be reasonable due to a large seismic array (more than 34 seismic stations triggered), however, the coverage is not particularly good around the area of interest. Furthermore, location can be expected to be compromised due to rock mass wave velocity variations, and recorded waveforms of poor quality. A procedure was applied (Malovichko and Hobson, 2010a, 2010b) doing locations for P- and S-arrivals and velocity assumption, varying these parameters within an interval of confidence, hence giving a 'cloud' of possible locations subject to abovementioned errors. These are shown in Figure 2, and although a significant location error is evident, it does indicate the most probable hypocentres. The most obvious interpretation from this is that the events are associated with the faults indicated by the fault loss (i.e. the Zuipings-type faults), and triggered by current mining adjacent to the faults.

Figure 2 Seismic event locations from a view accounting for Z error. The crosses are the best locations, while the dots represent possible locations by varying P- and S-arrivals as well as velocities

2.2.2 Source mechanism

Routine seismic moment-tensor analysis is difficult for the current scenario for a number of reasons. The most important factor is that seismic stations are distributed planar, hence not covering the source region well in three dimensions (i.e. the same reason as for large vertical location error). Furthermore, in practice a major problem arises with the orientation and response of sensors. In contrast to national and global seismological seismic networks, mine seismic systems are installed and run in harsh conditions. Proper installation of sensors may be compromised due to the constrained underground excavations. Furthermore, with time the response of the sensor may be distorted due to damage inflicted by heat and pressure, and also damage to the sensor cable. It also happens that during routine maintenance the component cables can be swopped resulting in incorrect orientation characteristics. The importance of sensor orientation verification in a study of seismic sources is emphasised in a paper of Julia et al. (2009), related to another South African deep level gold mine.

Recent work by Malovichko (2010), allowed for improved confidence for the sensor characteristics. The work is based on analysis of seismic signals from the following three types of seismic events:

- Local normal, small and medium size events
- Local mining blasts
- Distant large events (originating outside of the seismic network).

Comparison of the recorded amplitudes of seismic signals with the observed ones (from known source parameters) makes it possible to check the response of individual components. Calculation of misfit between polarisation of motion in P-wave and direction to the source enables a verification of the orientation. The orientation of a triaxial sensor may even be inverted by means of minimisation of such misfits for a set of events distributed around the sensor.

Applying the corrected sensor orientations allowed for more reliable moment-tensor results for the two seismic events of interest, which could be tested against the interpretation that the events are due to shear slip on the faults as suggested by their locations. This procedure considered a number of aspects which are not discussed in detail here, including the possibility of other potential sources in the area, alternative locations and slip directions, and implosive versus double-couple mechanism.

The beach-ball representations of the moment-tensor solution are shown in Figure 3a and 3b. It was concluded that the double-couple component included in the full moment-tensor was consistent with shear slip on the faults, with normal slip as could be expected for the Zuipings type faults. However, the most important conclusion was drawn from the relative contributions of different mechanisms to the full moment tensor. For the M3.0 event the main contribution was double-couple normal slip with minimal volume change (55 versus 16%). However, for the M4.0 the results suggest a small double-couple component (21%) with a significant isotropic component (66%). These conclusions are to be tested against observations and are described in the next section. As will be described later on, the numerical modelling addresses only the shear slip component of the seismic moment tensor and calibration will be about correlation between modelled and inferred double-couple shear slip.

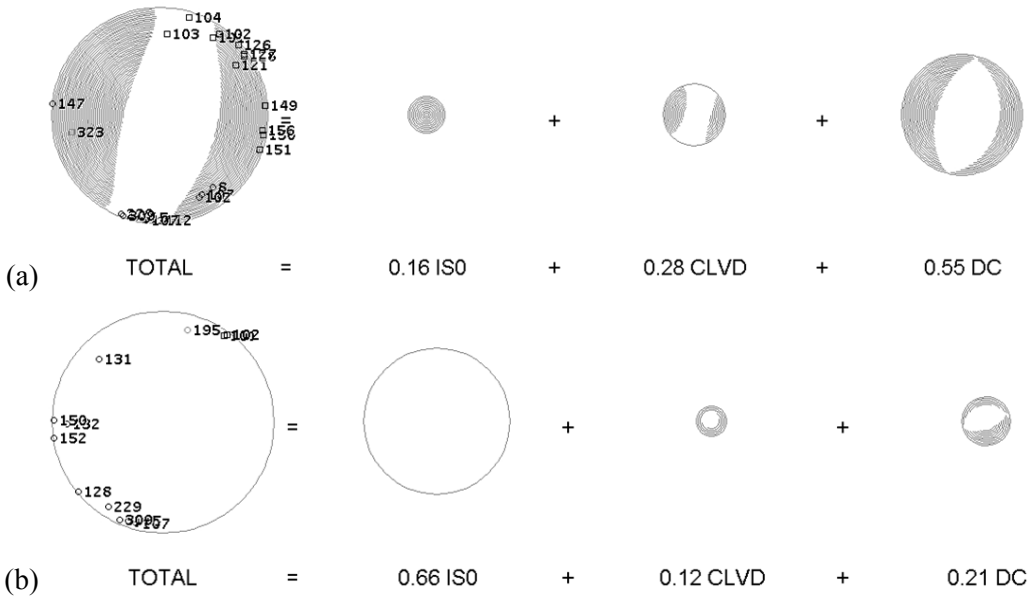

Figure 3 Beach-ball representations of the inverted mechanisms, also giving the relative contributions to the total seismic moment by the isotropic (ISO), compensated linear vector dipole (CLVD) and double-couple (DC) components: a) M3.0 seismic event of 15 October 2009; b) M4.0 seismic event of 29 November 2009

2.2.3 Source parameters

The most important estimate is seismic moment, which is accepted as a reasonable estimate of source deformation. Although scalar seismic moment is usually estimated assuming pure double-couple radiation and random coverage of the focal sphere, the values given here are based on the moment-tensor decomposition shown in Figure 3, and should be a more accurate estimate of the full scalar seismic moment. Table 1 gives this seismic moment together with some other source parameter estimates.

Table 1 Seismic source parameter estimates (Malovichko and Hobson, 2010a, 2010b)

	M3.0 Seismic Event of 15 October 2009	M4.0 Seismic Event of 29 November 2009
Seismic moment (Nm)	7.0E12	3.0E14
Radiated energy (J)	1.8E8	2.0E9
Energy S/energy P	13.6	10.9
Source size (m) (Brune source diameter)	210	511

2.3 Damage observations

The observed seismic damage to underground excavations gives an indication of both the source of a seismic event and the rock mass response to dynamic loading conditions associated with the event. It must be noted that the potential for damage in an excavation is inversely proportional to the distance from the source of the event and proportional to the 'size' or magnitude of the event, according to ground motion attenuation. However, damage is also driven by the rock mass response; i.e. highly stressed areas are more likely to be damaged than de-stressed areas. Furthermore, ground conditions and installed support also influences the rock mass response. Therefore all these issues must be taken into account in the process of interpreting the source of the event.

Historically at Great Noligwa Mine and in fact all the Vaal River area shafts, the access excavations have been more prone to seismic damage than the stopes. This can be associated with the scattered mining environment where the access ways are often positioned in stressed abutments on major geological features.

This is also true for the 64 Level travelling way leading to the mining area affected by the M3.0 event of 15 October. The damaged area next to the mining abutment corresponds with the high stress zone associated with that abutment. Coincidentally this is also the area where less effective dynamically ductile support had been installed.

The damage observed in the 64 travelling way is consistent with a far-field event (on the Zuipings fault). Significantly more damage would be expected if the excavation was inside the seismic source region. The observed damage may be explained as a secondary event/events triggered by the transient stress increase associated with the radiation from the source.

Damage observed in-stope is consistent with severe shaking of the stope due to transient seismic waves. Loose blocks were shaken from the hangingwall, but significant footwall damage was observed. Relatively little co-seismic closure occurred at the time of the event, indicating that the stope was not part of the event source. Bursting of in-stope pillars also occurred, confirming a high transient stress in either the hangingwall or footwall. The damage on the siding footwalls underneath the packs is consistent with this view.

With the M4.0 of 29 November, significant damage occurred at two crosscuts intersecting the Zuipings-B North 2 fault. Even though no direct evidence of slip on the fault was observed (no slip surface exposed) the damage in the crosscuts were focussed in a zone around the intersections with the Zuipings fault, indicating that this fault is the likely source of the event.

With this event the in-stope damage in the proximity of the Zuipings fault was significant with a large area completely closed (hangingwall on footwall). Some accelerated quasi-static closure has reportedly been observed prior to the event, but in excess of 1 m of co-seismic closure occurred at the time of the event. This is consistent with an event in the near field; i.e. the closure (footwall heave) is associated with slip on the fault.

The damage observed appears to confirm the Zuipings faults as the seismic sources, and the modelling back-analysis dealt with simulating shear slip on these faults.

3 Modelling methodology and input information

3.1 Boundary element model

Reef geometry and mined out areas were inferred from the best information available (reef blocks, contours and on-reef pegs). Monthly mining advance was incorporated from the beginning of 2009. Figure 4 is a detailed view of the area of interest, showing the monthly model steps together with development, mapped and inferred geology, etc.

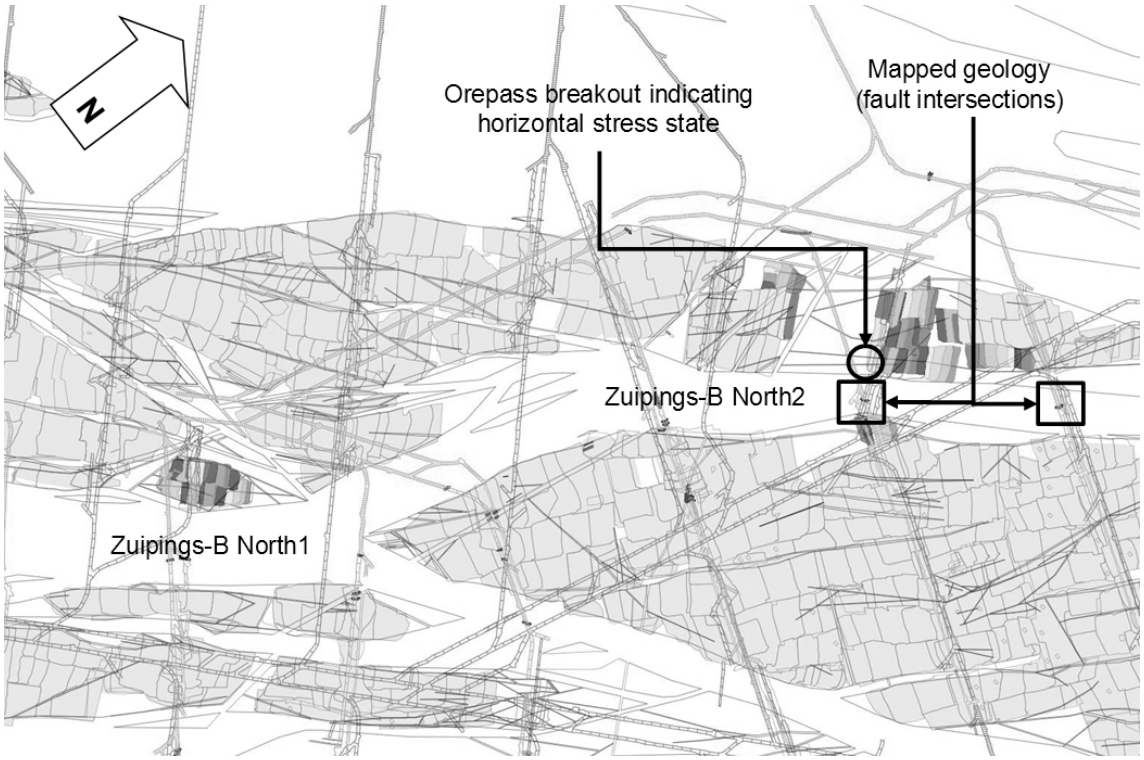

Figure 4 Plan view of the back-analysis area where the M3.0 and M4.0 are evidently associated with the Zuipings-type faults, in this case referred to as the 'Zuipings-B North 1 Fault' and 'Zuipings-B North 2 Fault'. Monthly mining steps from January to November 2009 and geological information are also indicated. The approximate dip of the faults is 50° as inferred from the throws between the reef blocks

Geological information indicated fault intersections (especially crosscuts around the area of interest) but no specific information was available of whether the intersections was Zuipings type faults, the strike and dip of the faults at intersections, or fault throws. Therefore a visual inspection of reef blocks turned out to be the best information on the dips of the Zuipings faults in the area, and a good fit was obtained for a dip of 50°. This suggested a single fault surface between mined out areas, assuming that historical mining 'stripped' against the fault. This interpretation also fitted fault intersections at a number of places (e.g. the ones indicated in Figure 4. Also indicated is the fault loss area of the two faults believed to be the seismic sources (from seismic locations), while Figure 5 shows perspective views of the undulating surfaces.

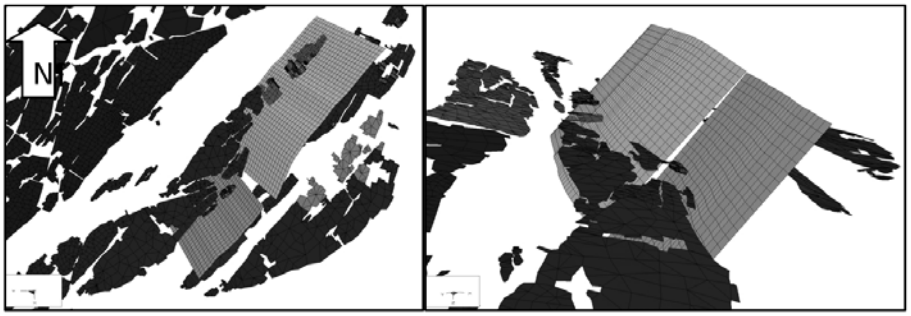

Figure 5 Perspective plan and section views of the structure geometries, as implemented in the boundary element model

Although shear slip seismic sources may be more complicated than single slip surfaces, it is assumed that the major forces driving shear slip over an extended surface can be simulated by using a single discontinuity surface.

3.2 Stress state

Various sources of information were used to infer best information on in situ stress state:

- A SIMRAC report by Stacey and Wesseloo (1998) evaluated available surface stress measurements across the mining regions of Southern Africa over the past 30 to 40 years. This indicated that for southern Africa the common trend of horizontal stress is northwest — southeast and northeast — south west, with the former mentioned orientation applicable for the Klerksdorp and Carletonville regions. A k-ratio of approximately 0.9/0.5 also appears to be applicable for both regions.
- A consultancy report conducted by ISS International Ltd (Lachenicht, 2000) considered ore pass scaling in the GNM shaft pillar, and generally the long axes of ore pass damage was observed to be in an east-west orientation. A worst-case k-ratio of 1.0/0.5 was used for assessing the future stability of the ore passes.
- Following the occurrence of the M4.0, the area was visited and an ore pass from 64 to 68 level could be viewed at the bottom of the raise. The orientation of the ore pass deformation was sketched and photographed. Although not measured quantitatively, the observations suggested a maximum horizontal stress orientation of approximately 15° west of north. This information is shown in Figure 6. The photograph down the ore pass was taken attempting to keep the camera aligned with the raise orientation, and therefore identifying the breakout orientation relative to the raise line. Although the photograph is not clear (due to limited flash range in total darkness), with some image processing it is possible to identify the ore pass shape, and from this determining the breakout line deviating approximately 15° west from north as indicated.

A further assumption was that the major principal stress was oriented orthogonally onto the reef plane, due to stress rotation under slip of bedding planes, driven predominantly by gravitational loading. At Tau Tona Mine (also a South African tabular deep level gold mine) stress measurements were done, confirming such an orientation of the major principal stress.

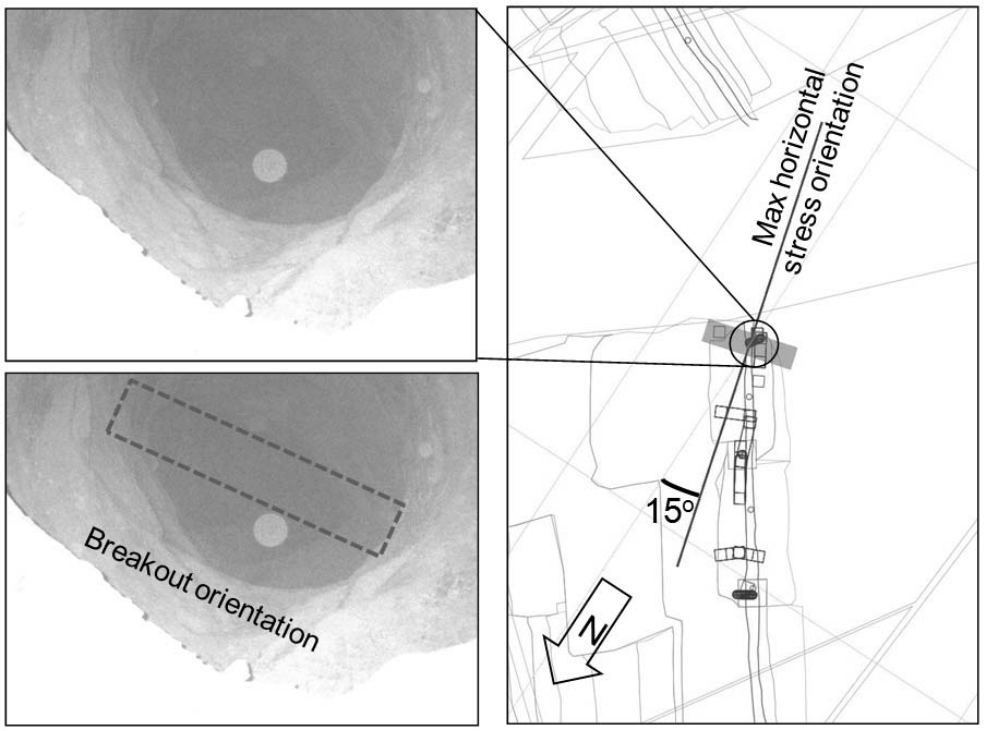

Figure 6 Underground observation used to infer horizontal stress orientation at the area of interest. The photograph was taken looking down into the orepass and keeping the camera parallel to the raise. The mine plan picture is at the same orientation, and the maximum horizontal stress orientation deduced is indicated relative to north

The abovementioned sources of information agreed, and a stress state consistent with that was deduced as follows:

- Host rock density 2,700 kg/m^3
- K-ratio NS/EW 0.9/0.5 (i.e. in terms of Cartesian stress components σ_{xx}, σ_{yy} and σ_{zz})
- Sigma1 ~ orthogonal to reef plane (with reef plane strike 42° and dip 20°)
- Datum 522 m.

3.3 Calibration parameters

Underground observations, the seismic locations, and reef block geometry around the area of interest suggest that the Zuipings-B faults are the sources of the M3.0 and 4.0 events. The most likely mechanism is shear slip, driven by mined out areas at the down-throw and up-throw sides of the fault, leading to a double-couple mechanism.

Calibration entailed firstly confirming whether the model simulates the supposed source mechanism, and secondly finding fault strength parameters providing a plausible slip area and amount of slip. This procedure towards calibration of the model is described below, starting with the parameters considered from a seismic and modelling point of view.

3.3.1 Modelled non-linear ride

Using the boundary element model and stress state described above, strength parameters of the structures were sought providing a source slip area consistent with the actual seismic events. Co-seismic slip can be simulated by non-linear ride, i.e. shear displacement on the structure boundary elements as a result of the shear stress exceeding the shear strength. Shear strength is based on the Mohr–Coulomb failure criterion, characterised by the friction angle and cohesion.

The condition for slip is therefore defined by the excess shear stress (ESS) criterion:

$$ESS = \tau - (C + \mu\sigma_n) \quad (1)$$

Where:

τ = the magnitude of the shear stress, $C + \mu\ \sigma_n$ is the shear strength, and C the contact cohesion.

μ = the friction coefficient.

σ_n = the normal stress ($\sigma_n > 0$ imply compression).

The Mohr–Coulomb criterion postulates that slip should occur where ESS is positive, or in the case of modelling, that non-linear ride will be simulated for positive ESS boundary elements. Furthermore, the model also takes as input the residual values of fault strength parameters, i.e. for friction angle (trigonometric arctangent of friction coefficient) and cohesion. Up to the point of shear failure (when ESS is negative) for a given boundary element, the peak friction angle and cohesion is used. When failure occurs (when ESS becomes positive), the residual values are taken, and in this way simulating strain softening when the peak strength is reached. The residual values are lower than the peak values, and hence more slip will occur once elements have started to fail. Apart from the amount of slip, the model also simulates stress transfer to other areas along a fault, which is also relevant for structure seismic hazard assessment.

3.3.2 Seismic potency

Traditionally the calibration of fault slip was done in terms of seismic moment, as an indication of deformation in the seismic source (Kostrov and Das, 1988). The numerical model provides estimates of shear slip on fault boundary elements, and modelled seismic moment can be calculated according to the interpretation scalar seismic moment:

$$M_o = GA\bar{D} \quad (2)$$

With:

M_o = the seismic moment.

G = the rigidity or shear modulus (GPa).

A = the source area.

$\bar{D}$ = the weighted average displacement.

However, for the purposes of comparing modelled slip with estimated shear deformation in the source from seismic waveforms, there is no need to refer to the shear modulus, which is an assumption anyway. From a seismic point of view, seismic potency P is given by:

$$P = A\bar{D} \text{ (in units of } [m.m^2]) \quad (3)$$

For a shear slip source, from which seismic moment can be calculated if the shear modulus is known. This is discussed in Mendecki (2005) as being a more reliable, and evidently more objective, estimate of deformation in the seismic source.

Jager and Ryder (1999) used the same concept for shear slip seismic source, referring to it as Volume of Ride:

$$V_R = \sum_i a_i.d_i \quad (4)$$

with a_i and d_i the areas and displacements of individual fault segments comprising the full fault slip area. This is calculated easily from numerical modelling results since the area and ride of individual fault boundary elements are given as model output.

Seismic potency can therefore be compared directly with modelled volume of ride (V_R) for purposes of calibration, with the units simply that of volume [m^3]. Seismic potency is directly proportional to seismic moment, and if required, the Hanks-Kanamori moment magnitude (M_{HK}) can be calculated, with this related

to local magnitude (subject to the fact that no information on slip velocity or seismic energy is known). For reference, Table 2 gives some example values of the abovementioned parameters.

Table 2 Example values of seismic moment and seismic potency, and the various relevant magnitudes in use in South African gold mines

M_{HK}	Typical Local Magnitude M_L	Seismic Moment M_o [Nm]	Log(M_o)	Seismic Potency P [m^3]	Log(P)
-1.0	-2.2	4.47E+07	7.65	0.001	-2.83
0.0	-0.8	1.41E+09	9.15	0.047	-1.33
1.0	0.5	4.47E+10	10.65	1.489	0.17
2.0	1.8	1.41E+12	12.15	47.085	1.67
3.0	3.1	4.47E+13	13.65	1,488.945	3.17

3.3.3 Displacement profile source model

Apart from calibration of fault strength to yield modelled seismic potency corresponding to the recorded values, it is also required to have some correlation between the source slip area and slip distribution across the fault surface. Although it is possible to perform so called source inversion from seismic waveforms to estimate the spatial slip distribution, this is not a trivial process. A so-called *displacement profile source model* is used here, from estimates of maximum displacement, source area and a theoretical displacement profile across the source area (Hofmann et al., 2001). It is assumed that the maximum displacement occurs at the event hypocentre (on the fault surface), and a taper function is used (i.e. a smooth decreasing function) to distribute displacement from the centre towards the edge of the source area. The generalised shape of the source area is assumed to be elliptical, which is an approximation of normal faults slipping along an extended strike span, driven by the tabular mining excavations under mainly gravitational loading. Although this is an idealised source slip distribution, it is used as a model of displacement across the fault that can be compared to modelled ride from the boundary element model.

The input information required for the displacement profile source model is the following:

- Maximum displacement D_{max}
- Taper function used for the displacement profile
- Source shape (defined by the ellipse eccentricity).

The estimate for maximum displacement is taken from Somerville (McGarr and Fletcher, 2003), giving D_{max} as a function of seismic potency P:

$$D_{max} = 0.0046 \sqrt[3]{P} \text{ (for a Rigidity of 30 GPa)} \quad (5)$$

For a set of input parameters seismic potency is therefore calculated for the displacement profile source model from the areas and displacements of individual segments on the fault surface (similar to modelled slip).

4 Back analysis and model calibration

4.1 Fault strength assumptions

The available input information does not allow for the derivation of a unique set of model parameters providing correlation between observations and model results. The approach is therefore to start with the best information on in situ stress state and structure geometry, and then to find fault strength parameters for the assumed stress state and structures providing plausible simulations of the sources of the two back-analysis seismic events. As discussed above the shear strength is defined by the peak and residual values for friction angle and cohesion, and appropriate values were sought for the two faults.

Literature and previous modelling experience was used as a guideline. Ryder (1988) suggested using a peak friction angle $\varphi_P = 30°$, from laboratory testing of quartzite. For modelling fault slip at Great Noligwa Mine, it is believed that that this value should be lower (faults weaker than brittle shearing of quartzite), and previous modelling assumed a peak friction angle $\varphi_P = 25°$ and residual friction angle $\varphi_R = 20°$. These values were therefore used as a starting point. The residual cohesion value was assumed to be $C_R = 0$, implying that all internal strength is lost during dynamic fault slip (also assumed by Ryder, 1988). Furthermore, the assumption was made that the same friction angles (peak and residual) are applicable for the two faults, implying that the fault surface roughness are similar, hence resulting in the same frictional shear strength caused by normal stress clamping. The remaining parameter is then peak cohesion, and it was assumed that this internal strength can be expected to be different for the two faults.

With changes in modelled surface stress, typically increase in shear stress, the onset of slip on fault boundary elements is determined by peak cohesion and friction angle. These values were therefore adjusted to yield sudden non-linear ride along the faults more or less at the mining stage when the two seismic events occurred. It was found that non-zero peak cohesion is necessary to simulate the 'sudden' co-seismic slip. Advancing mining causes an increase in ESS across the fault surface, possibly over a large area. At some stage, ESS for some elements will become positive, and in the boundary element model, those elements slip plastically. This result in shear stress transfer to surrounding elements and an 'avalanche' effect can ensue, causing a number of fault elements to slip, with these elements being close to the critical stress prior to that mining stage. Such a model of shear slip seems conceivable considering how large mining tremors are triggered by minimal mining.

A value for peak cohesion higher than previously thought was found to be applicable. Ryder (1988) stated peak cohesions of up to 10 MPa, but in this modelling analysis it was determined as around 16 to 20 MPa. The slip surfaces and timing of the seismic events in question could be simulated using such high peak cohesion. It turned out that a high peak cohesion also restricted slip mainly to the reef horizon, in particular between the up- and down-throw reef blocks in the current scenario, which seems more realistic than simulating slip far away from the reef horizon.

The next consideration is then the amount of slip of fault boundary elements, with seismic potency calculated by the sum of slip of all elements involved. This in turn is determined largely by the residual friction angle and cohesion values used in the model. An element will slip due to being driven by shear stress, and the resisting forces, i.e. dynamic shear strength (quantified by residual friction angle and cohesion) determines the amount of slip. Therefore, by again changing the residual strength values, modelled seismic potency can be calibrated with the recorded values for the events.

Numerous model runs were done testing different combinations of friction angle and cohesion, and it was concluded that peak friction angle $\varphi_P = 25°$ and residual friction angle $\varphi_R = 22°$ are appropriate, with a peak cohesion C_P around 16 to 20 MPa. These parameters yielded modelled seismic potencies of the same order of the recorded values for the two seismic events, and also simulated the co-seismic slip at the correct mining stage. These aspects are discussed in the following two sections.

4.2 Simulation of source mechanism

Figure 7 is an orthogonal view onto the structures, showing the modelled induced ride as solid contours for three model steps, i.e. the monthly mining stages during which the large events occurred. Only displacement values of greater than 1 mm are considered, assuming that such displacement will comprise the major source deformation and also taking this as a cut-off for calibration purposes.

At September 2009 (Figure 7a) the modelling suggests that large areas on the faults slipped historically, while minimal slip are modelled adjacent to the areas where mining was taking place at the time. Then, for the October mining step (Figure 7b) a relatively large area on Zuipings-B North 1 Fault slipped due to ESS, defined in terms of the peak friction angle and cohesion, becoming positive for some elements. Fault slip induced by the October mining step is depicted in Figure 7d, with this interpreted as a simulation of the seismic source of the M3.0 event of 15 October. Quantification of the weighted sum of model non-linear ride over the slip area can then be interpreted as seismic potency, and can be compared with the recorded potency associated with a double-couple mechanism. The model also provides the slip direction as indicated by the

arrow in Figure 7d. Similarly, the modelling indicates a large area on the Zuipings-B North 2 Fault slipping with the November mining step as shown in Figure 7c, with the induced slip shown in Figure 7e.

The proposed simulation of source mechanism seems plausible for the following reasons:

- Slip is restricted to the area on the fault between the down-throw and up-throw reef blocks, hence the conceivable double-couple mechanism expected for fault slip in this environment.
- Slip direction can be visualised in the boundary element modelling results, and this indicates normal slip as would be expected for the formation of these faults.
- The effect of mining excavations on potential for fault slip can be understood by visually considering the model geometry in 3D (i.e. extended mining spans close to the faults).
- The lobes of induced ride appear to be realistic source slip areas, approximately circular and elliptical for these two cases.
- Significant damage occurred at two tunnels intersecting the Zuipings-B North 2 Fault with the M4.0, spatially coinciding with the intersections of these tunnels with the fault, with significant fault slip modelled at these areas.

4.3 Quantification of modelled co-seismic slip

As discussed in the previous paragraph co-seismic slip for the two seismic events can be modelled using the boundary element model, albeit a representation of the static stress changes and corresponding induced slip. This is due to non-zero cohesion on the fault, since the contribution of cohesion to fault strength is independent of normal and shear stress. The ESS for a patch on the fault can therefore increase gradually as normal and shear stresses change with advancing mining, with the stress dependent shear strength approaching the constant cohesion. In this way a large area on the fault can reach a critical stress state, and when an element fails eventually, it can lead to stress changes on surrounding elements causing them to fail as well.

The model cohesion values were therefore refined to simulate the co-seismic slip at the actual mining stage. It was needed to manipulate the peak cohesions in order for the fault segments to slip at the mining stage that they did. However, this is justifiable due to fault components conceivably being of different cohesive strengths, most likely attributable to different ages and in-filling material. The following peak cohesion values were found:

- Zuipings-B North 1 Fault: C_P = 19.4 MPa
- Zuipings-B North 2 Fault: C_P = 16.1 MPa.

The remaining fault strength properties for both faults are:

- Residual cohesion C_R = 0 MPa
- Peak friction angle φ_P = 25° and residual friction angle φ_R = 22°.

These properties were applied for a model containing monthly mining steps since the beginning of 2009. A spatial filter was used to delineate the area of fault slip according to the model, and within which surface stress and ride is quantified. These results are given in Table 3. The first result of interest is potency induced per mining step. For the spatial filters some elements will fail in the model for the months before, but major slip is modelled for the months of October and November on the North 1 and North 2 faults respectively, i.e. when the large events occurred. The sudden modelled slip is interpreted as co-seismic fault slip, and seismic potency, slip areas and maximum slip can be calculated.

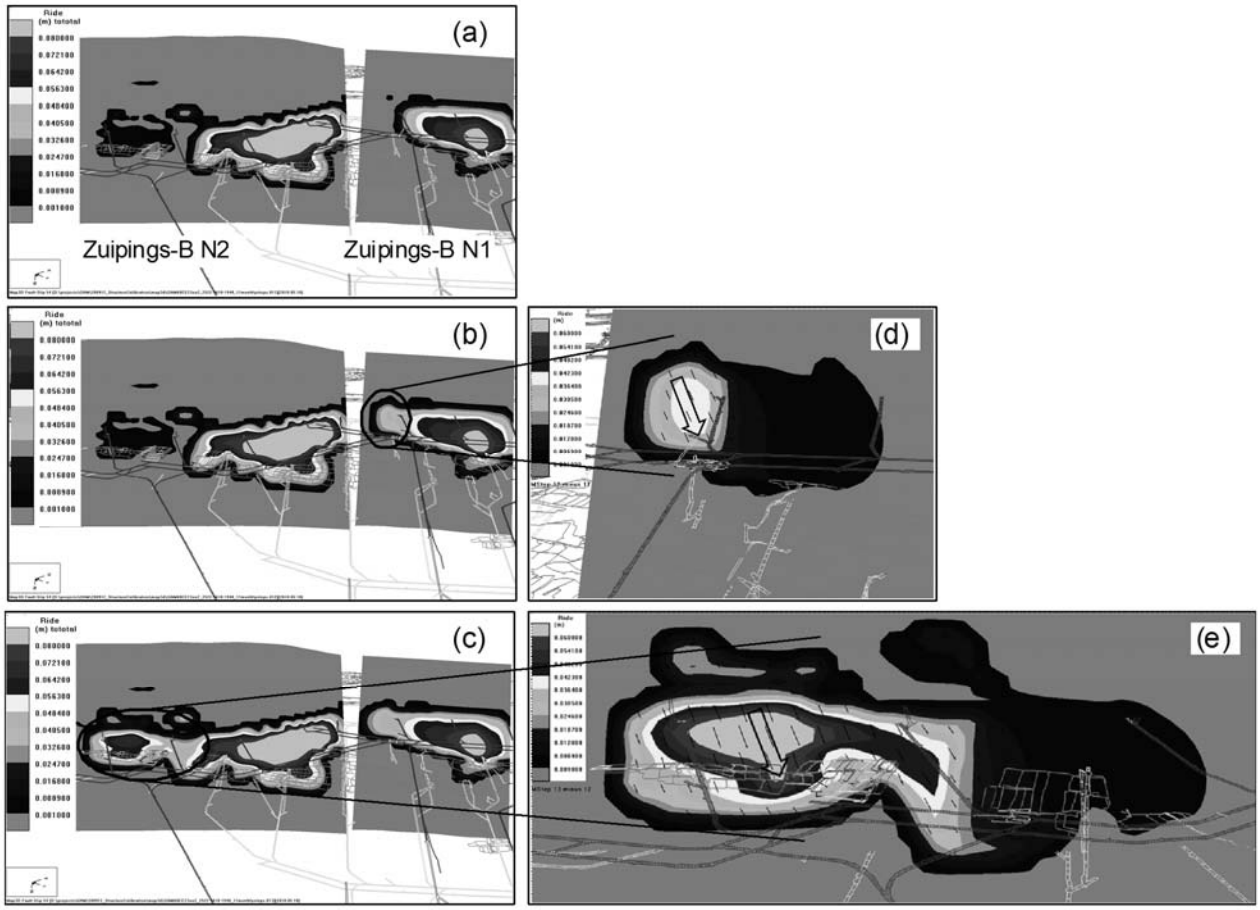

Figure 7 Orthogonal view onto the structures (looking approximately south) showing modelled ride for three model steps, i.e.: (a) September 2009; (b) October 2009; (c) November 2009. The October and November steps represent the mining steps when the M3.0 and 4.0 occurred respectively. (d) and (e) show the induced ride for the October and November steps, that are interpreted as the co-seismic source shear slip areas for the two seismic events

4.3.1 Seismic potency

Table 3 gives the data of induced seismic potency in the column named 'Pot_Ind'. For the M3.0 event a seismic potency value of 370 m^3 is modelled, compared to the recorded value of 233 m^3. For the M4.0 a seismic potency of 1,731 m^3 is modelled, compared to the recorded value of 10,000 m^3. The initial calibration effort attempted to find better correlation between the modelled and recorded values, but it became evident that such correlation could not be attained, especially for the M4.0 event, in which case a too small slip area was indicated by the modelling, and also by considering the mining geometries. However, it is suggested here that the isotropic (volume change) component of the source mechanism contributes a significant fraction to the total seismic potency. This is qualitatively in agreement with the isotropic versus double-couple mechanism shown in Figure 3b, and also the underground observations of co-seismic stope closure. The moment-tensor results indicate that a large fraction of recorded seismic potency for the M4.0 event was generated by stope closure, namely 66%, while 21% is attributable to double-couple, i.e. 2,100 m^3, compared with the modelled value of 1,731 m^3.

For the M3.0 event the double-couple mechanism contributes 55% to the total seismic potency, i.e. 128 m^3 of the total of 233 m^3, compared with the modelled value of 370 m^3. The results suggest modelled seismic potency of the right order of magnitude, considering the possibility that stope closure, which is not quantifiable by this boundary element methodology, can also contribute significantly to the total recorded seismic potency. For the two events the interpretation of co-seismic stope closure is also in agreement with the underground observations — minimal closure for the M3.0 event but significant closure with the M4.0.

McGarr (1999) reports on seismic events in the South African deep level tabular mining, and states that all of the 16 events considered were of normal faulting mechanism, but that 11 thereof contained a significant implosive component.

It is not proposed here that an absolute calibration of fault strength providing exact prediction of size and time of imminent large seismic events is attainable. Rather, this back analysis show that the main source mechanism for potentially damaging events in this environment is readily understood and can be modelled, and motivates the use of the suggested methodology and parameters for forward modelling.

Table 3 Modelling results on seismic potency induced (Pot_Ind) and associated maximum displacement (maxDispl). Some estimate of average shear and normal stresses along the source area is also given (Ave_w_SigS and Ave_w_SigN), reflecting the surface stress changes leading up to the large seismic events

Fault spatial filter = Zuipings-B North1					
Mining Step	Tot_Area [m²]	Pot_Ind [m³]	MaxDispl [m]	Ave_w_sigS [MPa]	Ave_w_sigN [MPa]
End 2008	2.267e+04	51.11	0.033239	21.4058	39.6549
09/01	2.267e+04	0.07	0.000044	21.4278	39.6662
09/02	2.267e+04	0.21	0.000130	21.5231	39.7457
09/03	2.267e+04	0.40	0.000278	21.7213	39.9079
09/04	2.267e+04	30.32	0.019839	21.6685	40.0859
09/05	2.267e+04	0.21	0.000080	21.7358	40.1305
09/06	2.267e+04	0.80	0.000314	22.0359	40.3511
09/07	2.267e+04	0.30	0.000128	22.1743	40.4653
09/08	2.267e+04	39.13	0.019771	22.1105	40.6916
09/09	2.267e+04	7.20	0.013487	22.2356	40.8405
09/10	**2.267e+04**	**370.32**	**0.04194**	**19.3690**	**40.8164**

Fault spatial filter = Zuipings-B North2					
Mining Step	Tot_Area [m²]	Pot_Ind [m³]	MaxDispl [m]	Ave_w_sigS [MPa]	Ave_w_sigN [MPa]
End 2008	6.955e+04	109.94	0.051370	23.8377	47.1107
09/01	6.955e+04	11.63	0.017635	23.9581	47.1599
09/02	6.955e+04	26.08	0.019784	24.0067	47.2011
09/03	6.955e+04	7.21	0.015230	24.1696	47.2488
09/04	6.955e+04	3.55	0.014165	24.4141	47.4391
09/05	6.955e+04	15.95	0.017861	24.3814	47.2993
09/06	6.955e+04	3.57	0.014387	24.3981	47.2293
09/07	6.955e+04	9.06	0.015206	24.4428	47.2316
09/08	6.955e+04	19.78	0.020564	24.5606	47.2858
09/09	6.955e+04	45.05	0.023349	24.6990	47.3595
09/10	6.955e+04	42.20	0.021887	24.7470	47.3854
09/11	**6.955e+04**	**1730.53**	**0.073175**	**21.4341**	**47.2475**

4.3.2 Maximum displacement

The numerical results also provide estimates of maximum co-seismic slip — the 'MaxDispl' column of Table 3, which can be compared with the estimate of Equation (5). Maximum slip for the M3.0 event derived from recorded seismic potency is estimated at 3.44 cm, compared with modelled co-seismic slip of 2.83 cm. For the M4.0 event, maximum slip from recorded potency is estimated at 9.91 cm, compared with modelled slip of 7.32 cm. However, it may be argued that only the double-couple seismic potency should be used for estimating maximum slip, in which case maximum displacement is estimated at 2.32 cm and 5.89 cm for the M3.0 and 4.0 respectively.

During the underground investigations no measurable fault slip could be observed to confirm above estimates. However, the damage was mainly to excavations in proximity to the faults and tunnels intersecting the faults, supporting shear slip on the faults as a significant part of the source mechanism.

4.3.3 Source size

The area of modelled induced slip was also compared with the displacement profile source model discussed in 3.3.3. It is required to assume a taper profile and a source shape (i.e. ellipse eccentricity), and the estimates of maximum slip is taken from seismic potency. A source slip area is then deduced comprising the full recorded seismic potency, i.e. assuming all is associated with shear slip. Slip distribution can then be visualised to compare with the source area from modelling, but Figure 8 shows only the elliptically shaped outline of the displacement profile source model for clarity.

It can be seen that the area of major modelled slip corresponds well with the displacement model for the M3.0 event — roughly a circular shape of diameter 170 m (Figure 8a). The shape can be understood considering the mining geometry — new mining at the down-throw side of the fault with the old mining at the up-throw side of the fault. It is important to note that the modelled event hypocentre, i.e. maximum slip, is some distance away from the new mining, supporting the minimal stope closure that occurred.

For the M4.0, the modelled induced slip area is much smaller than assuming that all recorded seismic potency is associated with shear movement (Figure 8b). Such a seismic event would have had a strike span of approximately 800 m according to the displacement profile model. Furthermore, in this case the maximum slip is in close proximity to the latest mining areas at the down-throw side of the fault, suggesting an increased potential for stope closure associated with the shear movement.

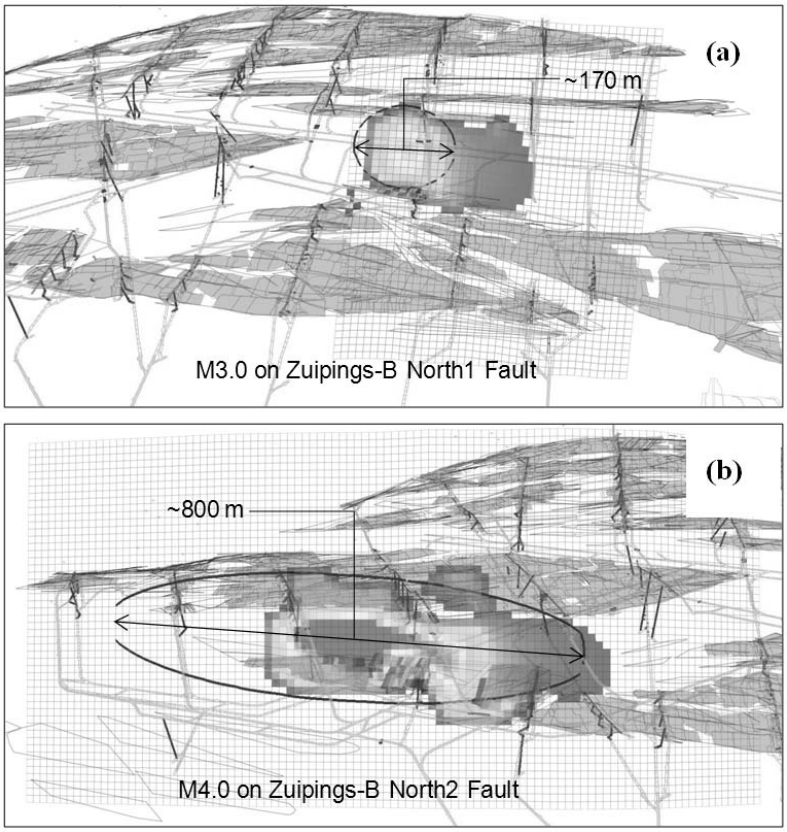

Figure 8 Orthogonal view onto the structures (looking approximately south) to compare the modelled induced ride with the displacement profile source model. The feint grids are the boundary elements representing the fault. The solid contours are induced modelled ride for the step at which the fault slips, while the ellipse indicates the source size according to the displacement profile, yielding seismic potency of the same amount as recorded, and assuming the maximum displacement coinciding with the modelled ride. Note that for the M4.0 (a) the area of slip suggested by the numerical model (solid contours) is significantly smaller than the displacement source model assuming that all seismic potency is associated with shear slip (ellipse). For the M3.0 (b) though, the source sizes are similar for the two models

4.4 Model sensitivities

The accuracy given for the peak cohesion values (19.4 and 16.1 MPa respectively) was required for the simulation of co-seismic slip at the specific mining steps. This has implications for implementing the proposed methodology to assess planned mining, since although strengths for these two faults was inferred, it can be expected that for other seismic events, whether on similar faults or other geological structures, cohesion will be different. It will not be feasible to attempt a back analysis on all large seismic events using the same approach, since this is a cumbersome process, and seismic sources will not always be well understood. However, it is believed that modelling parameters can be derived from this analysis providing a worst-case scenario in terms of the potential for damaging seismic events, and as such be used for assessing seismic hazard associated with planned mining.

A more undesired aspect however is that the modelling results presented here is also sensitive to the model geometry. During the back-analysis it became evident that building of mined and fault elements should be done carefully, in particular regarding grid size used for the fault surface and intersections between mining and fault elements. Although the general mechanism and fault slip area was stable, it was found that different fault element sizes result in fault slip at different mining steps. It has to be stated therefore that the peak cohesion required to simulate the co-seismic slip is dependent on the fault grid size, and cannot be taken as an absolute value. However, it is believed that high cohesion values are necessary to simulate slip as was demonstrated in this paper. For this analysis fault boundary element of square shape was used, with side lengths between 10 and 20 m. A further geometrical factor is fault elements in close proximity to mining elements, causing the unrealistically high elastic abutment stresses, also influencing results significantly. This required consistently maintaining a distance between fault and mining elements, and avoiding any intersections. A distance of 5 to 8 m was found appropriate, and careful model building was done in this respect.

The approach for forward modelling is therefore to apply a number of rules regarding model building, in addition to using the appropriate modelling parameters. An advantage of constant grid size on faults and no intersections with mining elements is that surface results can also be interpreted better due to more consistent contours, e.g. of modelled ride. This is not about a more pleasing picture, but for using the modelling as a tool to study potential slip areas on faults, and hence more efficient seismic hazard assessment.

It is the authors' opinion that the observed unstable model behaviour due to sensitivity to model parameters and geometry relates to why seismic tremors are so unpredictable.

5 Conclusions

A methodology is described here using static boundary element modelling to simulate seismic tremors associated with fault slip in a particular mining environment. Input information could be inferred with a fair level of accuracy, including the in situ stress state, general fault surface orientation from mined out areas, and monthly mining advances. Furthermore, although seismic source studies are always subject to the 'health' of the seismic system and adequate coverage, effort was spent in this case on the seismic location and moment-tensor inversion, and extracting best information from the recorded waveforms. For both seismic events underground investigations were also performed providing information on the faults involved and mining areas affected. The numerical modelling then entailed careful model building of the faults and mining geometries, and calibration of the strengths of the fault contacts believed to be the seismic sources. The modelled seismic source was consistent with double-couple normal fault slip believed to be the most likely mechanism in this tabular mining environment.

The analysis suggests that non-zero peak cohesion for faults is necessary to simulate potential slip effectively, with values of between 16 and 20 MPa found appropriate. However, this cannot be taken as absolute values since it is sensitive to model geometrical issues. For the seismic events considered here the modelled slip and slip direction provided a plausible source mechanism, viz. normal double-couple slip due to reef blocks offset by the historical throw on the fault. Such a source mechanism is in agreement with damage observations, as well as the area along the fault likely to be activated by mining in proximity. Regarding quantitative estimates of seismic potency, the model provided satisfactory estimates of the recorded values. However, it was found that for fault slip a significant fraction (potentially exceeding 50%) of total seismic potency released may be due to stope closure. Efficient moment-tensor analysis may assist in

understanding historical seismic events, but for forward analysis the unknown imminent mechanism may result in underestimation of seismic potency. The location of the modelled lobe of ride relative to mining excavations does provide a clue though, in that modelled maximum slip close to mining may result in a significant stope closure component, and hence higher levels of damage.

Application of the proposed methodology and modelling parameters will require accurate model building, including geometrical surfaces of faults using the best information available. In situ stress state is naturally a crucial input, with this determining surface shear and normal stresses, and hence excess shear stress leading to fault slip. Careful examination of results will also be required, towards understanding how the stress state, mining geometry and structure geometry can lead to large seismic events. Knowledge gained from the model can then be used in the mine planning process, through identification of seismic hazards relative to mining excavation and access tunnels.

Acknowledgements

The contribution of ISS International is greatly appreciated, in particular D. Malovichko who performed the seismic analyses presented here, for diligently submitting consultancy reports and for informative discussions. The involved staff of Great Noligwa Mine is thanked (especially J. Oelofse and G. Kotze), for assistance with the underground visits, collating information and discussions.

References

Hofmann, G., Sewjee, R. and Van Aswegen, G. (2001) First steps in the integration of numerical modelling and seismic monitoring, in Proceedings Dynamic rock mass response to mining, 5th International Symposium, G. Van Aswegen, R.J. Durrheim and W.D. Ortlepp (eds), Camera Press, Johannesburg.

Jager, A.J. and Ryder, J.A. (1999) A handbook on rock engineering practice for tabular hard rock mines, The Safety in Mines Research Advisory Committee (SIMRAC), Creda Communications, Johannesburg.

Julia, J., Nyblade, A., Durrheim, R., Linzer, L., Gök, R., Dirks, P. and Walter, W. (2009) Source Mechanisms of Mine-Related Seismicity, Savuka Mine, South Africa, Bulletin of the Seismological Society of America, Vol. 99, No. 5, pp. 2801–2814.

Kostrov, B.V. and Das, S. (1988) Principles of earthquake source mechanics, Cambridge University Press.

Lachenicht, R. (2000) Orepass Stability Assessment at Great Noligwa Mine, ISS International Ltd Project Report, Document No GNM-REP-010.

Malovichko, D. (2010) Great Noligwa Mine: System Diagnostics and Sensor Orientation for the period 2010 January – 2010 March, ISS International Ltd consultancy report, Document No ISSREP_GNM_SYSDIAG201003_v1.

Malovichko, D. and Hobson, S. (2010a) Great Noligwa large event report: M3.1, 16h07 on 15 October 2009, ISS International Ltd consultancy report, Document No ISSREP_GNM_LRGEVT20091015-M31_v2.

Malovichko, D. and Hobson, S. (2010b) Great Noligwa large event report: M4.0, 04h04 on 29 November 2009, ISS International Ltd consultancy report, Document No ISSREP_GNM_LRGEVT20091129-M40_v1.

McGarr, A. and Fletcher, J.B. (2003) Maximum Slip in Earthquake Fault Zones, Apparent Stress, and Stick-Slip Friction, Bulletin of the Seismological Society of America, December 2003, Vol. 93, No. 6, pp. 2355–2362.

McGarr, A. (1999) On relating Apparent Stress to the stress causing earthquake fault slip, Journal of Geophysical Research, Vol. 104, No. B2, pp. 3003–3011.

Mendecki, A. (2005) Persistence of Seismic Rock Mass Response to Mining, in Proceedings Sixth International Symposium on Rockburst and Seismicity in Mines (RaSiM6), Y. Potvin and M. Hudyma (eds), 9–11 March 2005, Perth, Australia, Australian Centre for Geomechanics, Perth, pp. 97–106.

Ryder, J.A. (1988) Excess Shear Stress in the assessment of geologically hazardous situations, Journal of the South Africa Institute of Mining and Metallurgy, Vol. 88, No. 1.

Stacey, T.R. and Wesseloo, J. (1998) Evaluation and Upgrading of Records of Stress Measurement Data in the Mining Industry, Safety in Mines Research Advisory Committee – Final Project Report for GAP 511b.

Wiles, T. (2010) Map3D User's Manual, Mine Modelling Pty Ltd - www.map3d.com, Australia.